Tribology International 184 (2023) 108476

Contents lists available at ScienceDirect

Tribology International

journal homepage: www.elsevier.com/locate/triboint

Tribo-induced catalytically active oxide surfaces enabling the formation of the durable and high-performance carbon-based tribofilms

Kim Khai Huynh [a], Sang T. Pham [a,b,*], Anh Kiet Tieu [a,**], Sean M. Collins [b], Cheng Lu [a], Shanhong Wan [c]

[a] School of Mechanical, Materials, Mechatronic and Biomedical Engineering, University of Wollongong, Wollongong, NSW 2522, Australia
[b] School of Chemical and Process Engineering, School of Chemistry, and Bragg Centre for Materials Research, University of Leeds, Woodhouse Lane, Leeds LS2 9JT, UK
[c] State Key Laboratory of Solid Lubrication, Lanzhou Institute of Chemical Physics, Chinese Academy of Sciences, Lanzhou 730000, PR China

ARTICLE INFO

Keywords:
Carbon tribofilms
Layered double hydroxide
Lubricant additives
Tribocatalytic
Catalytic active surfaces

ABSTRACT

Carbon-containing tribofilms have attracted significant interest in the lubrication research despite a scarcity of information on their high-temperature performance under severe boundary conditions. In this study, high-temperature lubrication of the carbon tribofilm produced from cyclopropane carboxylic acid (CPCa) and NiAl-layered double hydroxide (LDH) nanoparticles was evaluated. NiAl-LDH nanoparticles significantly enhanced the friction stability and antiwear performance of CPCa by over 90% at 50°C and 100°C, comparable to the benchmark zinc dialkyldithiophosphates (ZDDPs). The highly graphitic amorphous carbon tribofilms and the fine-grain intermediate tribolayer constructed by the thermal decomposition products of NiAl-LDH contributed to such excellent lubrication performance. This study paves a pathway in developing functional anti-wear additives for the durable and high-performance carbon-containing tribofilms at high temperatures.

1. Introduction

With the increase in transportation, the demand for efficiency in energy consumption and environmental safety is becoming essential [1]. To alleviate the adverse effects of climate change, the introduction of heavy-duty vehicles with electric or hybrid systems has been proposed with many promising prospects [2–4]. The fully-integrated electrical vehicles still require time to complete their full developing processes, and improving the energy efficiency in the internal combustion engine (ICE) still attracts significant attention. There are two approaches to optimize energy efficiency by controlling the friction and wear including the optimization of lubricant packages and the improvement of the contact interface by surface texturing or by the application of functional coatings [5]. Among these, enhancing engine oil performance is considered the more practical approach [1]. The main target is to formulate a new class of lubricants that can promote friction and wear reduction produced from the contacting surfaces inside the engine. Research of novel lubricant additives that not only improve the base oil lubricity but also minimise harmful elements like Phosphorus or Sulphur is essential [1,6,7].

To comply with the "green" requirements for efficiency contacting, the use of Diamond-like Carbon (DLC) as the carbon-based coating has emerged as a potential solution [1,2]. This kind of hard coating was first investigated by Schmellenmeier et al.[8]. Since then, numerous types of Carbon-based coatings have been further developed to adapt with the engineering requirements within engine systems [9,10]. Despite the proven lubricating functions, these coatings is still limited because of their restricted thicknesses and easy-delamination characteristic that will require re-deposition after a long time of operation [11]. To overcome these issues, Erdemir et al. [12] has introduced a novel method to promote in-situ Carbon-based tribolayer formation from base oil during sliding. The key mechanism of this approach is the utilization of the flash temperature and contact stresses to trigger the tribochemical reactions between the hydrocarbon molecules to form the solid carbon films [13–15]. By doping the hard sputtered coating with a metallic catalytic agent, such tribochemical processes can be achieved which resulted in excellent tribological performance, even superior compared to the zinc dialkyl dithiophosphates (ZDDPs) tribofilm in some conditions.

* Corresponding author at: School of Chemical and Process Engineering, School of Chemistry, and Bragg Centre for Materials Research, University of Leeds, Woodhouse Lane, Leeds LS2 9JT, UK.
** Corresponding author.
E-mail addresses: t.s.pham@leeds.ac.uk (S.T. Pham), ktieu@uow.edu.au (A.K. Tieu).

https://doi.org/10.1016/j.triboint.2023.108476
Received 28 January 2023; Received in revised form 22 March 2023; Accepted 2 April 2023
Available online 3 April 2023

Following the concept of Erdemir et al. [12], a novel pathway to develop functional coatings where several studies have been conducted to form the Carbon-based tribofilm from different carbon precursors, ranging from gas to liquid and to solid forms, by different metallic atoms with catalytic nature [16–18].

Another approach to generate the carbon films at the sliding contacts is by the use of lubricant additives, i.e. oil-soluble carbon-precursor additives constructing from the highly strained cycloalkane moieties, hydroxyl and/or carboxylic acid functional groups (e.g.) [19]. Compared to the hard catalytic coatings, this approach is more convenient since it does not require the pre-treatment and re-deposition of the coatings when the coatings are completely worn off. Cyclopropane carboxylic acid (CPCa) has recently been recognized as a promising candidate for this approach [20,21]. The carbon tribofilm is developed during sliding via the dissociation and polymerization of the cyclopropane moiety from this molecule [22,23] in conjunction with the absorption of the carboxylic group (-COOH) on the steel substrates [19,24]. The formation of this in-situ Carbon-based tribofilm at room temperature testing condition could improve remarkably the lubrication performance of the PAO-4 oil by reducing the wear rate by 93% and the friction by 18% [21]. However, an inferior anti-wear performance of CPCa compared to ZDDP was found in the previous study under strict boundary lubrication with limited supply of the lubricant during the test [25]. It has been hypothesized that the polymeric carbon-based tribofilm from CPCa could be rapidly sheared off under the boundary lubrication and it could not be replenished under the limited presence of CPCa when the testing duration was extended [21]. More importantly, the lubrication performance of this Carbon-based tribolayers at high temperatures has not yet been considered elsewhere.

Beyond the use of the carbon-precursor additives, current work done by Wang et al. [26] has recognized the potential of the layered double hydroxide (LDH) nanoparticles containing catalytically active metallic elements, e.g. NiAl-LDH, in forming the carbon tribofilms. LDH is a new class of layered materials that shows high potential in lubrication science due to their controllable sizes, shapes and compositions [27,28]. The simple, low-cost [29,30], and environmentally friendly [31] synthesis of LDH materials attracts significant interest for practical applications. Apart from their thin layered structure, which enables easy access to the solid's interfacing area and provides an excellent shearing capability, their nanometer size can fill in rough surfaces and reduce surface roughness, promote a tribofilm, and/or improve the fluid dynamics of the lubricant, which are the characteristic performances of the layered materials [32]. From the initial study [26], the lubricating effect of LDH nanoparticles was also attributed to the formation of the compact tribolayer comprising the nano-crystalline NiO and $NiAl_2O_4$. Noticeably, further research demonstrated the catalytic effect of the NiO phase formed from the thermal decomposition of NiAl-LDH in transforming the attached hydrocarbon molecules into solid carbonaceous materials [33,34]. These carbon products had a graphitic-like carbon structure that stayed around the NiO nanoparticles. From this perspective, catalytically active LDH nanomaterials exhibit significant potential for in-situ production of high-performance Carbon-based tribofilms.

In this study, we advanced the tribological performance of in-situ Carbon-based tribofilms produced from CPCa by the addition of NiAl-LDH nanoparticles. In particular, the friction and wear behaviour of the lubricant containing CPCa at different temperatures were evaluated, and the effect of NiAl-LDH nanoparticles in the enhancement of the CPCa lubrication was investigated. The tribofilm structures were fully investigated using advanced electron microscopy analysis to understand the synergistic behaviour of the NiAl-LDH in improving the formation of the high-performance of the Carbon-based tribofilms at the sliding interface. The collected information will be used to elucidate the lubrication mechanisms of the combination between LDHs and carbon-precursor additives, thus, evaluating their potential application in practical applications for wide temperature range.

2. Experimental section

2.1. Chemicals

SpectraSynTM4 PAO-4, denoted as PAO-4, base stock has a kinematic viscosity of the PAO-4 oil is 19 cSt at 40°C and 4.1 cSt at 100°C, and it was provided by ExxonMobil. Cyclopropane carboxylic acid (CPCa) and Zinc dialkyldithiophosphate (ZDDP) were purchased from Sigma-Aldrich Corporation (NSW, Australia) and Luoyang Trunnano Tech Co., Ltd. (Luoyang, China), respectively. $Ni(NO_3)_2.6H_2O$ was provided from the Scharlab lab sourcing group (Barcelona, Spain), while $Al(NO_3)_3.9H_2O$, Na_2CO_3, and NaOH were provided from Chem-Supply Pty Ltd (SA, Australia). All the chemicals were used without further purifications or modifications unless otherwise indicated.

2.2. Synthesis of NiAl-LDH nanoparticles

NiAl-CO_3 LDH was synthesized by the co-precipitation method described elsewhere [29]. Typically, 40 mL cation solution of $[Ni^{2+}] = 0.6$ M and $[Al^{3+}] = 0.3$ M was prepared by dissolving certain amounts of $Ni(NO_3)_2.6H_2O$ and $Al(NO_3)_3.9H_2O$ powders in distilled water. It was then added dropwise to a 20 mL anion solution of Na_2CO_3 3 M. A stream of 2 M NaOH, used as the basic agent, was added continuously to the solution to maintain the pH value of the mixture at 10 ± 0.5. The obtained solution was magnetically stirred for at least half an hour before being transferred into an autoclave for hydrothermal treatment for 15 h at 100°C. The autoclave was naturally cooled to room temperature before the Ni-Al-LDH precipitates were vacuum filtered from the suspension, washed with distilled water and ethanol several times, and dried for 12 h at 80°C. Finally, the dried cake was ground to a fine powder. The obtained LDH nanoparticles have the formula $[Ni_{1-x}Al_x(OH)_2](CO_3)_{x/2}.mH_2O$ with x = 1/3 in this study, according to the Ni/Al ratio equal to 2.

2.3. Formulating the lubricants

CPCa, an oil-soluble carbon tribofilm precursor additive, was blended to PAO-4 via magnetic stirring for 30 min. The concentration of CPCa in the base oil was kept at 2.5 wt% according to previous studies [21,25]. Subsequently, certain amounts of the fine NiAl-LHD powders were dispersed and ultra-sonicated in the formulated lubricant for 8 h while the temperature was maintained at 30°C by the cooling water bath. Prior to each test, the formulated lubricant was redispersed in an ultrasonic bath for at least 30 min to minimize any potential settling and agglomeration of the particles. Different amounts of Ni-Al-LDH added to the lubricant mixture were examined to find the optimum concentration of the LDH nanoparticles on the lubrication performance. The denotation of tested lubricants are listed in the following table: (Table 1).

The lubricant containing only NiAl-LDH and PAO-4 with no addition of CPCa did not form stable dispersions and was therefore not used for tribological testing. The appearance of accumulated solid (Fig. 1) evidenced the poor dispersion of NiAl-LDH in PAO-4 without CPCa added. A certain amount of NiAl-LDH (0.10 wt%) was ultra-sonicated in PAO-4 for at least 8 h with no additions of CPCa. The agglomeration and precipitation of the NiAl-LDH particles occurred rapidly after the ultrasonication ceased. This behavior could be strongly related to the

Table 1
Naming convention of the tested lubricants.

Test Lubricants	Denotation
PAO-4 oil	PAO-4
PAO-4 oil + 2.5 wt% CPCa	CPCa
PAO-4 oil + 2.5 wt% CPCa + x wt% NiAl-CO_3 LDH	CPCa+x%LDH
PAO-4 oil + 2.5 wt% ZDDP	ZDDP

x = 0.05, 0.07, 0.10, and 0.15

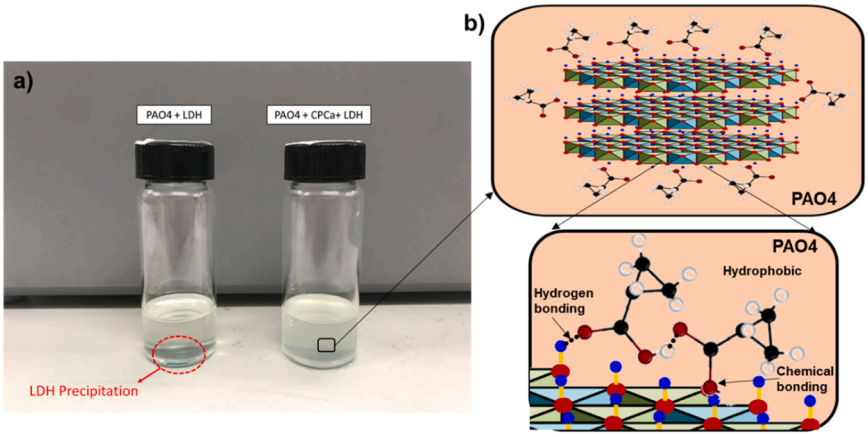

Fig. 1. Dispersibility of the synthesized NiAl-CO_3 LDH in PAO-4 oil with and without the presence of CPCa after 8-hour ultrasonication.

chemical structure of LDHs. In particular, the LDH crystal structure includes a layer of divalent and trivalent metal cations connected via exchangeable anions [35]. In every layer, each cation combines with -OH functional groups to form an octahedral structure where centred on the cation [36]. The presence of a large number of -OH functional groups on the cation layer of LDHs makes LDHs very hydrophilic, resulting in poor dispersion in non-polar media such as PAO-4 (Fig. 1a). Meanwhile, CPCa aids in dispersing the NiAl-LDH powder within the PAO-4 as the CPCa molecule is ampiphilic, containing two moieties: a highly strained cycloalkane and the surface-active -COOH functional group. Due to its amphiphilic nature, CPCa provides hydrophobic termination for the NiAl-LDH materials, supporting uniform dispersion in PAO-4. That is, the active -COOH group of CPCa can connect to the -OH groups on the LDH surfaces via chemical substitution (chemical bonding) or hydrogen bonding (Fig. 1b). Such interactions resulted in the chemical and physical adsorption of CPCa on the layers of LDHs with the cycloalkane moieties pointing toward the oil phase (Fig. 1b). Since the cycloalkane moieties are hydrophobic and are always dissolvable in oil, the CPCa-adsorbed LDHs can be dispersed well in oil-based lubricants.

2.4. Tribological experiments

The tribo-tests were performed on a Bruker Universal Mechanical Tester (UMT) instrument under unidirectional mode at a linear speed of 0.1 m/s with an applied constant load for an hour. A 6.35-mm diameter GCr15 (AISI 52100 grade) steel ball with 9.7 ± 0.2 GPa hardness [37,38] was held stationary to slide over a rotating 3 mm thick and 30 mm diameter bearing steel disc (AISI 52100 grade). The testing temperature was set at 25 °C, 50°C, and 100°C. Prior to the tribo-test, the rotating disc, with a hardness of 10.9 ± 1.3 GPa, was polished to the roughness $R_a = 252 \pm 41.5$ nm. The composition of the experimental tribopair can be found in Table 2:

Before the testing, the ball and disc were ultrasonically cleaned with hexane, acetone, and ethanol, respectively to wash away any contaminants on the disc and ball surfaces. All the tests were performed at least three times to ensure the repeatability and reproducibility of the friction and wear results. Prior to the friction and wear test, the fixed amount of lubricant (1 mL) was drop cast on the disc surfaces. There was no addition of new lubricant during sliding to imitate the shortage-supply conditions of lubricant additives. Different normal loads of 10 N, 20 N, and 30 N (corresponding to the Hertzian pressure of 1.26 GPa, 1.59 GPa, and 1.82 GPa, respectively) were tested to evaluate the load-bearing capability of the tested lubricants. According to Dowson–Higginson equations [39], the boundary lubrication regime for all tribo-tests was guaranteed. In particular, the minimum film thickness and lambda (λ) value for the selected conditions under 10 N normal load are $h_{min} = 23.75$ nm and $\lambda = 0.09$. The boundary lubrication regime and the shortage-supply conditions, which are together termed as severe boundary conditions, were selected to evaluate the stability and durability of the carbon tribofilms resulting from the tested lubricants. After the tribo-test, the ball and disc were cleaned with hexane, acetone and ethanol to remove any residual oil on the surfaces. The Contour GT-K 3D Optical Microscope was used to examine the wear loss volumes, and the wear rate was calculated using the Eq. (1):

$$\text{Wear } Rate = \frac{\text{Wear Loss } Volume(\text{mm}^3)}{\text{Applied Normal } Load(\text{N}) * \text{Sliding } Distance(\text{m})} \quad (1)$$

2.5. Characterization

The crystal structure of NiAl-LDH was characterized by using a mini-materials analyzer (MMA) X-Ray diffractometer. X-ray powder diffraction (XRD) patterns were acquired across a range of 5–70° range of 2θ angle using a copper Kα X-ray source with a 1°/minute scan rate and 0.02° step size. A 35 kV-maximum voltage was used to generate a 28.4-mA current. Scanning electron microscopy (SEM) was carried out using a JSM6490LV (JEOL, Japan) operated at 15 kV and a working distance of 10 mm and equipped with energy disperse spectroscopy (EDS) to observe the morphologies and element distribution of the tribofilms on the worn surfaces. Raman spectroscopy was performed using a Renishaw Raman spectrometer (Woltton-under-Edge, UK) to analyze the tribofilms on the wear surfaces, using a spot size of 10 μm and laser wavelength of 539 nm. Meanwhile, the cross-section specimens of the balls' wear surfaces were prepared using a focused ion beam–scanning electron microscope (FIB-SEM, Helios NanoLab G3 CX, Thermo Fisher Scientific, USA) with a liquid Ga ion source operated at 30 kV and 96 pA. Prior to the ion milling, the worn surfaces were deposited with protective layers of platinum and carbon, respectively to avoid milling-induced damage to the surface/subsurface layers. Bight field scanning transmission electron microscope (BF-STEM) and EDS elemental mapping were carried out by scanning transmission electron microscope (STEM)

Table 2
Experimental tribopair compositions.

	C	Mn	Si	P	S	Cr	Fe
Disc	0.93%	0.43%	0.24%	0.003%	0.008%	1.38%	Rest
Ball	0.95–1.05%	0.35%	0.25%	0.025%	0.025%	1.40–1.65%	Rest

using JEOL ARM 200 F STEM microscope equipped with a Schottky field emission gun source and operated at 200 kV. Electron energy loss spectroscopy (EELS) was also carried out by the same instrument to analyse the graphitic degree of the carbon-based tribofilms. High-resolution TEM lattice imaging and selected area electron diffraction (SAED) were performed by using Titan^3 Themis 300 (X-FEG source, 300 kV) to identify the compositions and phases of oxide interlayers, respectively.

3. Results

3.1. Characterization of the obtained LDH powder

Fig. 2 shows the characterization results of synthesized NiAl-CO_3 LDH material from SEM and XRD techniques. According to Fig. 2a, the obtained Ni-Al-LDH exhibited a flake-like structure with their lateral size mostly ranging within 40–60 nm. This observation indicates an effective synthesis process that resulted in NiAl-CO_3 LDH nanomaterial with an acceptable homogeneity. Besides, XRD analysis in Fig. 2b reveals a prominent reflection of several peaks at the 2θ of (003), (006), (110) and (113) diffractions which are characteristic of the layered structure of LDHs [40,41]. The sharp and narrow (003) and (006) peaks at 11.78^o and 23.62^o indicate the high crystallinity of the sample. According to Bragg's law [27], the interlayer *d*-spacing value was calculated as 0.752 nm for the obtained Ni-Al-LDH.

3.2. Tribological performance of the formulated lubricants at room temperature

Fig. 3 shows the friction and wear results of the sliding test under the normal load of 10 N at room temperature. According to Fig. 3a, PAO-4

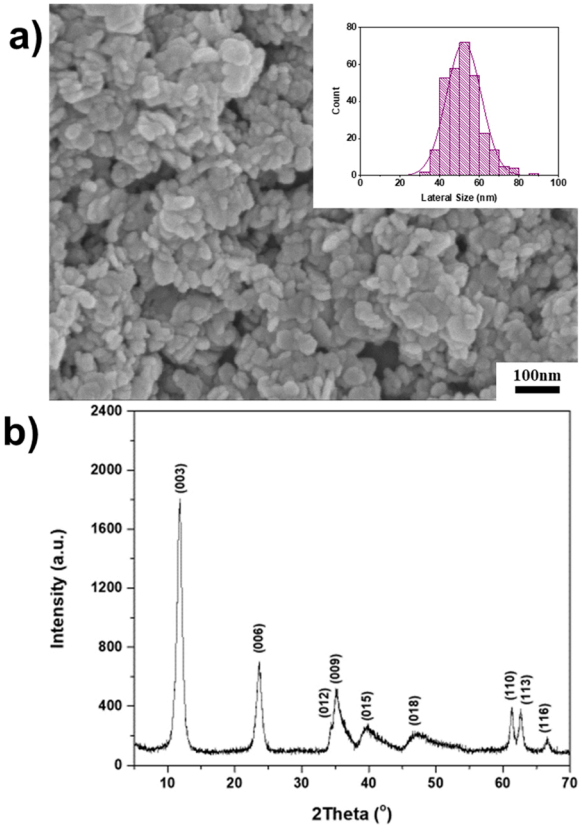

Fig. 2. Characterization of the synthesized NiAl-CO_3 LDH material: (a) SEM image observation. An inset picture is the lateral size distribution of the Ni-Al-LDH; (b) XRD pattern of the Ni-Al-LDH.

has the highest coefficient of friction (COF) of 0.12 at the steady state. The addition of 2.5 wt% CPCa to PAO oil reduced the friction and stabilized the COF at 0.08 for the first 20 min of the testing, but the friction showed a sharp increase to reach a steady-state friction value of PAO-4 in the last 40 min. This could indicate the rapid removal of the polymeric carbon-based tribofilm produced from CPCa under severe boundary condition due to the unstable absorption of this tribofilm on rough steel substrates [20,25]. Over the time, the CPCa was depleted during sliding and the polymeric carbon-based tribofilm could not be regenerated, thus, leading to an increase in friction.

Meanwhile, the combination between 2.5 wt% CPCa and 0.1 wt% LDH not only further reduced the friction value of CPCa after 20 min of sliding but also maintained a much lower friction outcome than PAO-4 until the tribotest ceased. The COF value at the steady state of this formulated lubricant was around 0.08 which is 33.3% lower than PAO-4. Moreover, this lubricant also produced the lowest ball wear rate of 1.4×10^{-8} mm^3/Nm, while the results from the lubrication of CPCa and PAO-4 are 2.7×10^{-8} mm^3/Nm and 11.7×10^{-8} mm^3/Nm, respectively (Fig. 3b). It is in agreement with the reduced roughness variation in the disc wear track lubricated by the CPCa+ 0.1%LDH compared to PAO-4 and CPCa (Table S2).

Besides, the tribotests with different NiAl-LDH concentrations in the formulated lubricants have highlighted 0.10 wt% as the optimum concentration that delivered the best tribological outcomes (Fig. S1-S2). The addition of NiAl-LDH less than 0.1 wt% did not improve effectively the friction and wear performances. A gradual increase in friction occurred, and eventually reached the steady-state value of PAO-4 after around 25-minute sliding which indicates the depletion of the tribofilms on the wear surfaces (Fig. S1a). There is also no significant reduction in the ball wear rate compared to CPCa when the concentration of NiAl-LDH was kept below 0.1 wt% (Fig. S1b). Meanwhile, the addition of 0.15 wt% Ni-Al-LDH reduced the friction outcome to 0.09 but this friction downtrend period only lasted for over 20 min before a sudden increase occurred. Compared to 0.1 wt% Ni-Al-LDH, the average wear rate with the 0.15 wt % test is slightly higher (Fig. S1b). It is anticipated that the Ni-Al-LDH started to agglomerate at 0.15 wt% leading to a decrease in lubrication performance. Thus, 0.10 wt% LDH was the optimum condition that was selected for further tribotest experiments.

Fig. 4 shows the SEM and EDS results of the ball wear scars from the tribotests of PAO-4, CPCa, and CPCa+ 0.1%LDH under 10 N load at room temperature (25°C). SEM, using the secondary electron detector, observation of the ball wear scar from PAO-4 reveals a flat wear surface with the presence of some abrasive scars (Fig. 4a). According to the EDS analysis, these scars are oxygen (O)-rich areas indicating a direct and continuous contact of large asperity or third-body abrasive particles during sliding. The flat wear surface on the ball could be due to the severe wear abrasion between the disc and ball which delaminated fully the rough tribo-oxide layer. Over the wear surface of the ball, the direct asperities contact occurred which resulted in a wide oxidation area under PAO-4 lubrication (Fig. 4a). The signal intensity of carbon (C) is also found on the wear surface which could come from the oil decomposition [25]. In the case of CPCa, the trace of carbon-based tribofilm formation can be observed via the presence of some low-contrast and carbon-rich clusters on the wear surface (Fig. 4b). The distribution of O over the wear surface is not uniform compared to the one obtained from the PAO-4 lubrication, suggesting the reduced oxidation degree at some local areas on the wear surfaces. There is an appearance of some grooves across the wear scar which indicates the presence of the third body wear particles that dislodged the polymeric carbon tribofilm produced from CPCa.

Intriguingly, the addition of NiAl-CO_3 LDH into the CPCa lubricant at the concentration of 0.1 wt% produced no abrasive wear marks or scratches on the sliding surfaces (Fig. 4c). It has been demonstrated that the formation of scratches and abrasive marks relates closely to the morphology, size, and shape of the added solid lubricant particles [42]. From the SEM image in Fig. 2a, the NiAl-CO_3 layered

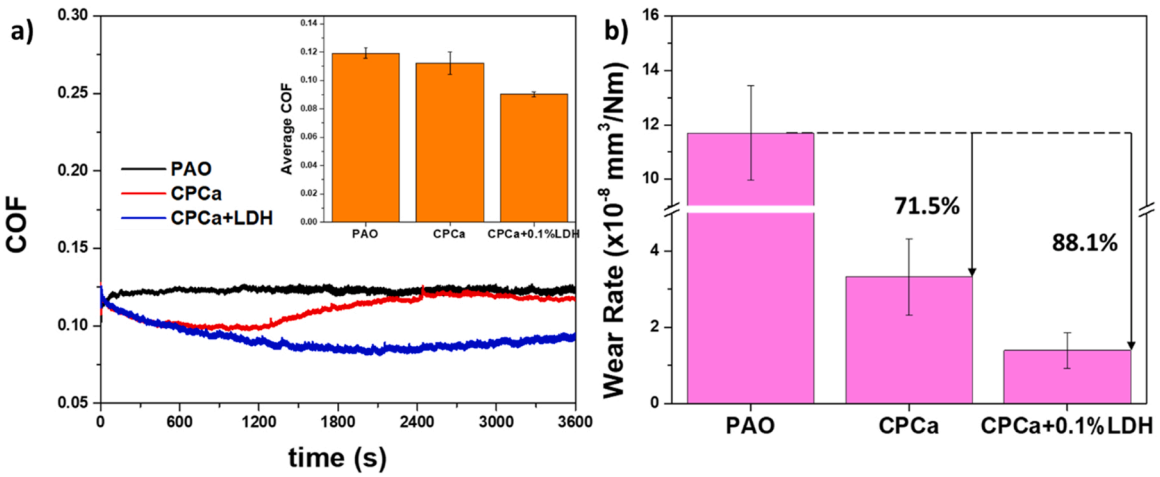

Fig. 3. Friction and wear results of PAO, CPCa, and CPCa+ 0.1%LDH under 10 N load at 25°C: (a) frictional curve and the average coefficient of friction (COF), and (b) average ball wear rate. The vertical axes break in (b) is to distinguish the wear rate resulted from the lubrication test of CPCa and CPCa+ 0.1% LDH.

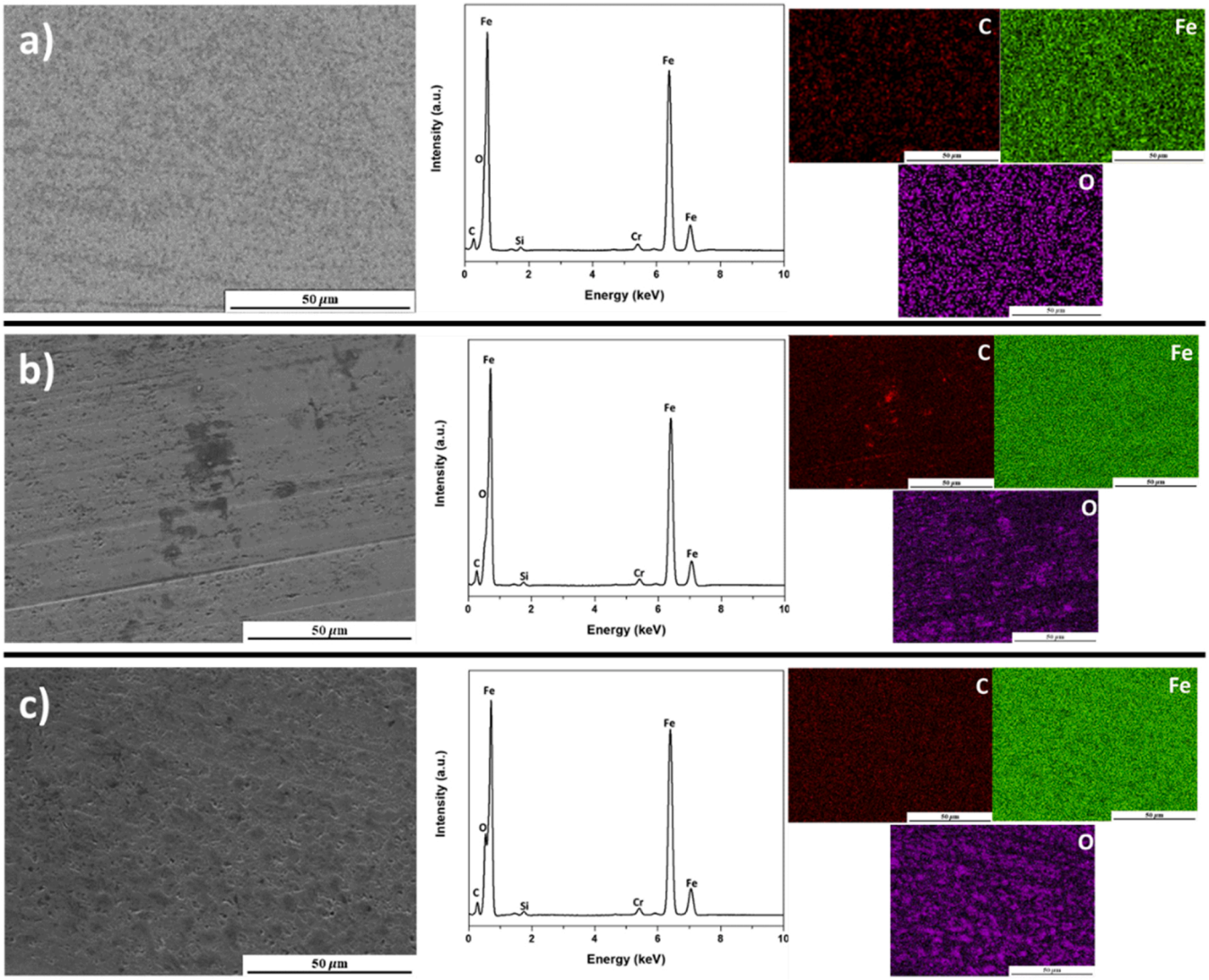

Fig. 4. SEM images and EDS results of ball wear scar (a) PAO-4, (b) CPCa and (c) CPCa+ 0.1%LDH under 10 N load at 25°C.

submicron-particles were rounded with no sharp edges which could not damage the lubricated rubbing surfaces. Rather, these particles were adsorbed and incorporated onto the sliding surface to play a protective role. However, EDS analysis, both spectrum and mapping, does not show the presence of aluminum (Al) and nickel (Ni) over the ball wear scar. This could demonstrate that there was no compact tribofilm formation at 25°C, and CPCa-modified NiAl-LDH nanoparticles presented between the sliding surfaces to separate the direct asperity contacts. The non-uniform distribution of O in the EDS mapping compared to that obtained from PAO-4 and even CPCa suggests that NiAl-LDH nanoparticles and CPCa molecules co-absorbed and formed a temporarily protective layer at some areas on the sliding surfaces which protected the wear surfaces from oxidation. It is interesting to note that the presence of NiAl-LDH could prolong the low-friction regime and further reduced wear damages (Figs. 3a-3b). Further tribotests with higher normal loads showed an outstanding load-carrying effect of such a protective layer up to 20 N in terms of wear damage protection (Fig. S3 and S4). More discussion on the lubrication mechanism of this physisorption protective layer at 25°C will be made in the discussion section.

According to Roberts et al. [43], the lubricant oil in a conventional combustion engine usually operates in the temperature range of 100°C-110°C. Nevertheless, most of the friction and wear loss comes from the initial warm-up stage where the temperature is around 20°C [44,45]. Furthermore, nearly 33% of vehicle trips do not heat the lubricant inside the system over 60°C [43,46]. As a result, when developing a new lubricant for engine applications, it is critical to ensure the lubricant can exhibit an acceptable performance under various operating temperatures while not producing any harmful emissions to the environment. The next sections dedicated to the investigation of the high-temperature lubrication performance of the CPCa and CPCa + 0.1 wt% NiAl-LDH additives in PAO-4 compared to the benchmark ZDDP additive, which is well-known for its excellent anti-wear property at high temperatures.

3.3. Dependence of tribological performance of the formulated lubricants on temperature

Figs. 5a-5b describes the friction and wear results of the formulated lubricants at 50°C. Accordingly, the friction curve from CPCa lubricant experiences a sharp increase from ~0.12 to ~0.15 after only 15 min of sliding. It then fluctuates around the steady-state average COF of ~0.14. Meanwhile, the CPCa+ 0.1%LDH exhibits a more stable COF behaviour around 0.125 after a mild variation in the first 25 min of sliding. The presence of Ni-Al-LDH stabilized significantly the friction performance of CPCa and reduced slightly the COF by 11.34%. The wear rate of CPCa+ 0.1%LDH lubricant is about 0.519×10^{-8} mm^3/Nm which is 94% lower than CPCa (8.68×10^{-8} mm^3/Nm) (Fig. 5b). It agrees with the disc wear surface after lubricating by CPCa lubricant showing a higher roughness variation than the one lubricated by CPCa+ 0.1%LDH lubricant at 50°C (Table S5). More interestingly, the combination of CPCa+ 0.1%LDH also exhibited superior anti-wear performance (by ~49.2%) compared to ZDDP at this temperature while the friction was also slightly lower.

At higher temperature (100°C), the CPCa+ 0.1%LDH lubricant still demonstrated its outstanding lubrication under 10 N. Fig. 5c shows the loss in anti-friction property of CPCa at 100°C which is evidenced by its

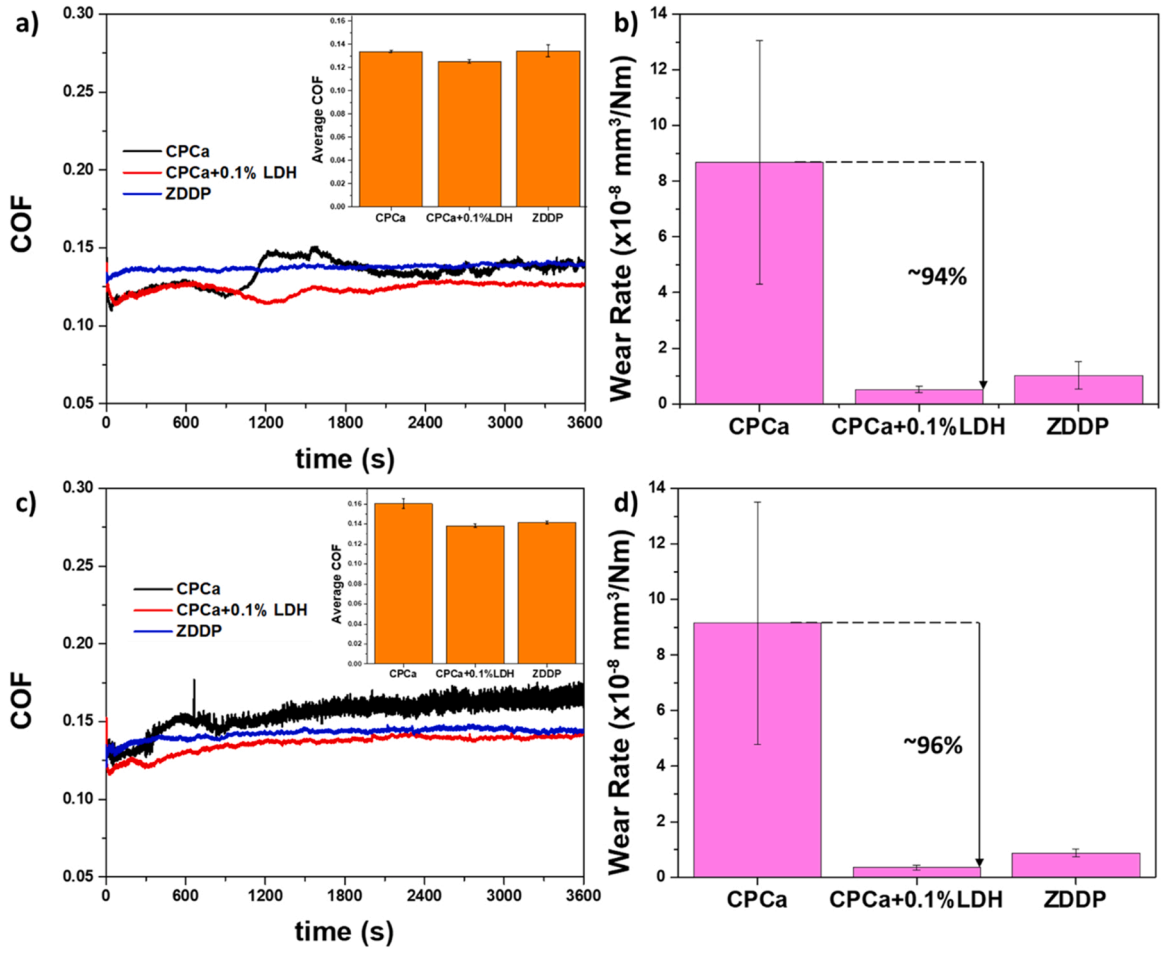

Fig. 5. Friction coefficient (a) and average wear rate (b) of CPCa, CPCa+ 0.1%LDH, and ZDDP lubricants under 10 N at 50°C. Friction coefficient (c) and average wear rate (d) of CPCa, CPCa+ 0.1%LDH, and ZDDP lubricants under 10 N at 100°C.

continuous increase with a high variation in the friction curve. The average COF at the steady-state of CPCa is estimated at around 0.16. With the presence of 0.1 wt% NiAl-LDH, the friction curve is more stable with little variation. It reaches the steady-state value of ~0.14 after 15 min of sliding. In addition, the CPCa+ 0.1%LDH lubricant also exhibited an outstanding anti-wear performance with a 96% lower wear rate (~0.35 × 10^{-8} mm^3/Nm) compared to that produced from CPCa lubricant (~9.15 × 10^{-8} mm^3/Nm) (Fig. 5d). It is in agreement with the reduced roughness variation in the disc wear track lubricated by the CPCa+ 0.1%LDH compared to CPCa (Table S6). Compared to the ZDDP lubricant, the CPCa+ 0.1%LDH lubricant still produced a moderately lower wear rate (by ~ 17.4%) with nearly equal friction behaviour at 100°C. These results demonstrated the outstanding lubricating function of CPCa+ 0.1%LDH at a wide temperature range, being comparable to the benchmark ZDDP additive.

Fig. 6 shows SEM and EDS results of the ball wear scar surfaces after lubricating by CPCa+ 0.1%LDH lubricant at 50°C and 100°C. Compared to the room testing condition (Fig. 4c), the wear surfaces obtained from the tribotests at 50°C show some scars. There are even various deep scratches across the wear surfaces at 100°C testing condition. This was due to the thinner lubricant at increasing temperatures which shifted the lubrication process into the more severe boundary lubrication regime. Under such a condition, the collision between the asperities becomes more significant which generally generates abrasive wear patterns. The wear scar produced at 50°C is rough with a wavy pattern where the presence of a minor abrasion scar is observed (Fig. 6a). However, unlike the results from room temperature, EDS mapping illustrates a uniform distribution of Ni and Al elements across the worn surface. Their presence was confirmed by the EDS spectrum integrated from whole field of view which shows distinguishable peaks of these elements compared to the one from room temperature tribotest (Fig. 4c). The C, Fe and O mapping also shows uniform distribution over the wear surfaces. The EDS results suggest the formation of a compact tribofilm at 50°C which could be constructed from the LDH elements, carbon film from CPCa, and oxide layer. On the other hand, the EDS mapping of the ball wear scar after testing at 100°C shows the local distribution of the Ni and Al as well as C elements over the wear surfaces (Fig. 6b). It is interesting that these elements with O distribute at the same areas over the worn surface where Fe shows weak intensity on the mapping. The entire wear surface shows the strong intensity of Ni, Al, C, and O which indicates that the compact tribofilm was formed over the wear surface during sliding at 100°C.

3.4. Raman examination of the wear surfaces at different temperatures

Raman analysis was used to characterize the chemical characteristic of the balls' wear surfaces lubricated by CPCa+ 0.1%LDH lubricant at different temperatures (Fig. 7). The ball lubricated at 25°C shows a strong intensity of the magnetite (Fe_3O_4) compared to hematite (Fe_2O_3) at 682 cm^{-1} and ~1306 cm^{-1}, respectively [47,48]. There are small peaks at ~1440 cm^{-1} and ~1660 cm^{-1} for CH_2 vibration and C═C stretching of the carboxylic acid and hydrocarbon [49], respectively, which suggest the residues from oil and/or CPCa molecules. There is no detection of the G band and D band from carbon tribofilm indicating that there is no carbon tribofilm on the wear surface. It is in good agreement with SEM-EDS analysis (Fig. 4c). On the other hand, the balls lubricated by CPCa+ 0.1%LDH lubricant at 50°C and 100°C show the presence of

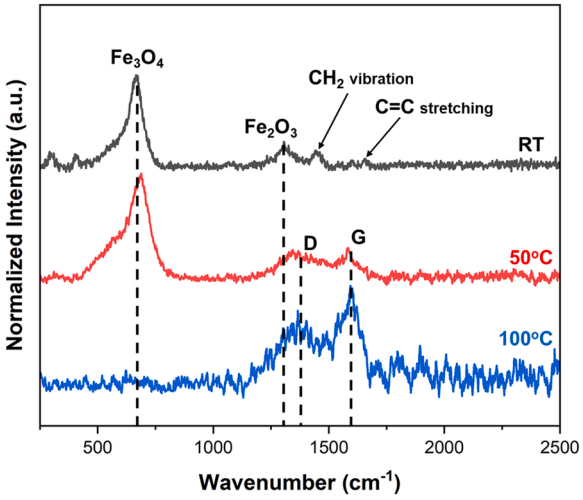

Fig. 7. Raman analysis of wear surfaces lubricated by CPCa+ 0.1%LDH lubricant under 10 N load at room temperature, 50°C, and 100°C.

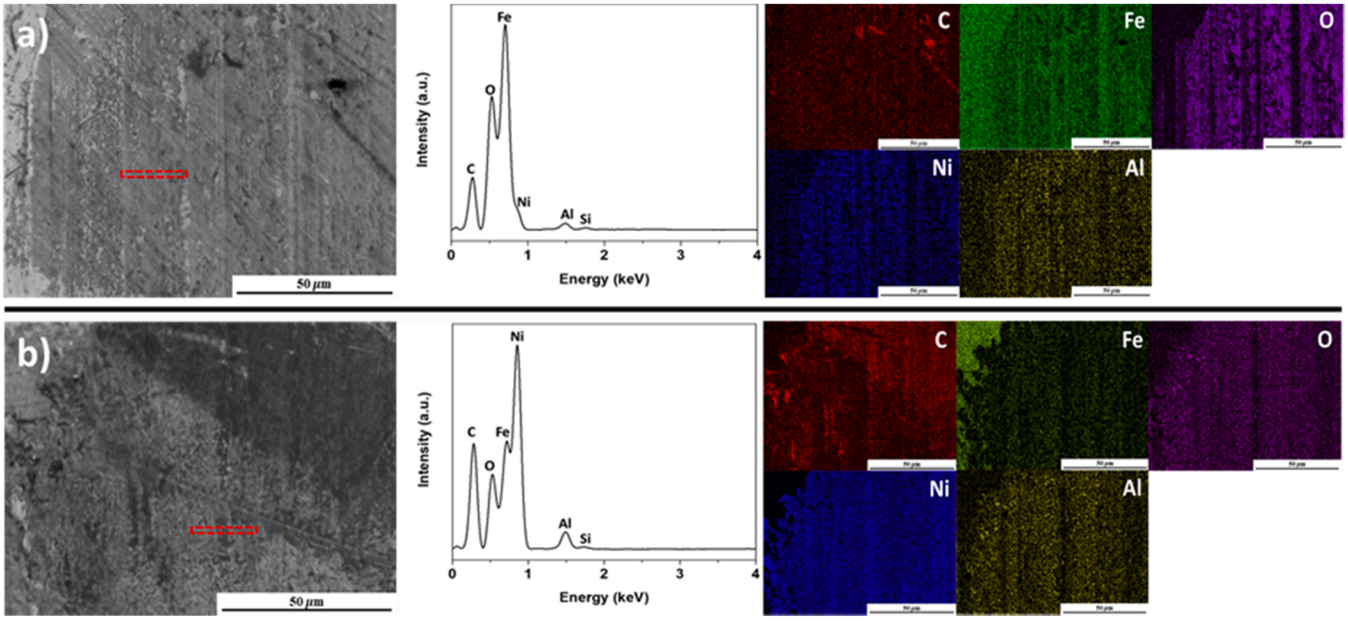

Fig. 6. SEM and EDS results of the ball wear scar surfaces lubricated by CPCa+ 0.1%LDH under 10 N at (a) 50°C and (b) 100°C. (The red rectangles in (a) and (b) indicating the areas for FIB milling).

the D band and G band in their Raman spectrum. In particular, the ball tested at 100°C shows only the presence of the D band and G band with the shape being similar to diamond-like carbon (DLC) in some areas. There are no peaks of iron oxides in such areas which could suggest the formation of a relatively thick tribofilm above the iron oxide layer. However, a recent report has proved that Raman could give false interpretations about the formation of the carbon tribofilm based on the Raman analysis [23]. The presence of the D band and G band in the Raman spectrum with a shape similar to DLC has been used widely to conclude the formation of the carbon tribofilm, but such Raman features of DLC can be formed by photochemical and thermochemical reactions of the carbonaceous materials triggered by the Raman laser [50]. Thus, further characterizations of the tribofilm, regarding both physical and chemical structures, were conducted in the next sections by STEM analysis.

3.5. Hierarchical structure of the tribofilms produced at different temperatures

To characterize the structure of the tribofilms on the wear surfaces, FIB milling was conducted to prepare thin lamellae for cross-sectional examination of the ball wear scars (Fig. 6a, 6b). Fig. 8a shows the formation of a bi-layer tribofilm on top of the steel substrate after testing at 50°C. An approximately 20 nm thick amorphous layer is found located above a 100-nm thick compact layer of small grains. From the STEM-EDS analysis (Fig. 8b), the amorphous superficial layer is carbonaceous material while the compact small grains layer shows the strong intensity of Ni, Al, Fe, and O. The compact small grains layer could be the mixed oxide tribolayer produced during testing by the oxidation of NiAl-LDH followed by the compaction with iron oxides. Core-loss EELS analysis was conducted at the top amorphous carbon film to reveal the chemical bonding state of carbon in the matrix (Fig. 8c). A sharp peak centring at 285.5 eV can be observed indicating the transitions to the π * molecular orbital due to the presence of sp^2 bonding [51]. The second, broader and more intense peak ranging between 290 and 292 eV, is induced by transitions to σ * orbitals [51]. The EELS spectrum obtained at three different regions, denoted as EELS1, EELS2, and EELS3, shows a similar shape which is characteristic of the amorphous carbon. Further calculation of the graphitization degree of the carbon tribofilm based on the concentration of the sp^2 bonding was carried out by using the integration window approach [48,52]. The calculation method was based on the previous study where the sp^2 bonding fraction is calculated by taking the division of the $\frac{I_{\pi^*}}{I_{\pi^*}+I_{\sigma^*}}$ ratio, obtained from the EELS spectrum in this study, over the $\frac{I_{\pi^*}}{I_{\pi^*}+I_{\sigma^*}}$ of the highly oriented pyrolytic graphite (HOPG) [51]. The ranges of energy window for sp^2 and sp^2+sp^3 are from 282 eV to 288.5 eV and 297 eV, respectively. Accordingly, the sp^2 fraction of the carbon tribofilms ranges between 66% and 72% for the spectra taken at three different areas (Fig. 8c). These values are significantly higher than the sp^2 fraction of the amorphous carbon film produced from oil decomposition [48] (c.a. 32%) which indicates an increase in the graphitic degree attributable to the tribofilm formation itself.

The composition and structure of the mixed oxide tribolayer beneath the carbon tribofilm are also of interest and this information was obtained by combining the STEM-EDS (Fig. 8b) and selected area electron diffraction (SAED) (Fig. 8e). Based on the chemical information in EDS and the indexing of the diffraction rings in SAED, the presence of NiO, Fe_3O_4, and Fe_2O_3 phases can be found in the mixed oxide tribolayer (Fig. 8b and 8d). The SAED pattern shows sharp diffraction rings characteristic of polycrystalline material which indicate that the tribo-oxide layer is the compaction of the fine grains. The faint halo ring pattern in the SAED can be recognized and it could be from the amorphous phase presenting in the tribo-oxide layer. From the previous study, the formation of the NiO was recognized as the thermal decomposition of NiAl-LDH nanoparticles under friction conditions at 50°C [26]. However, the

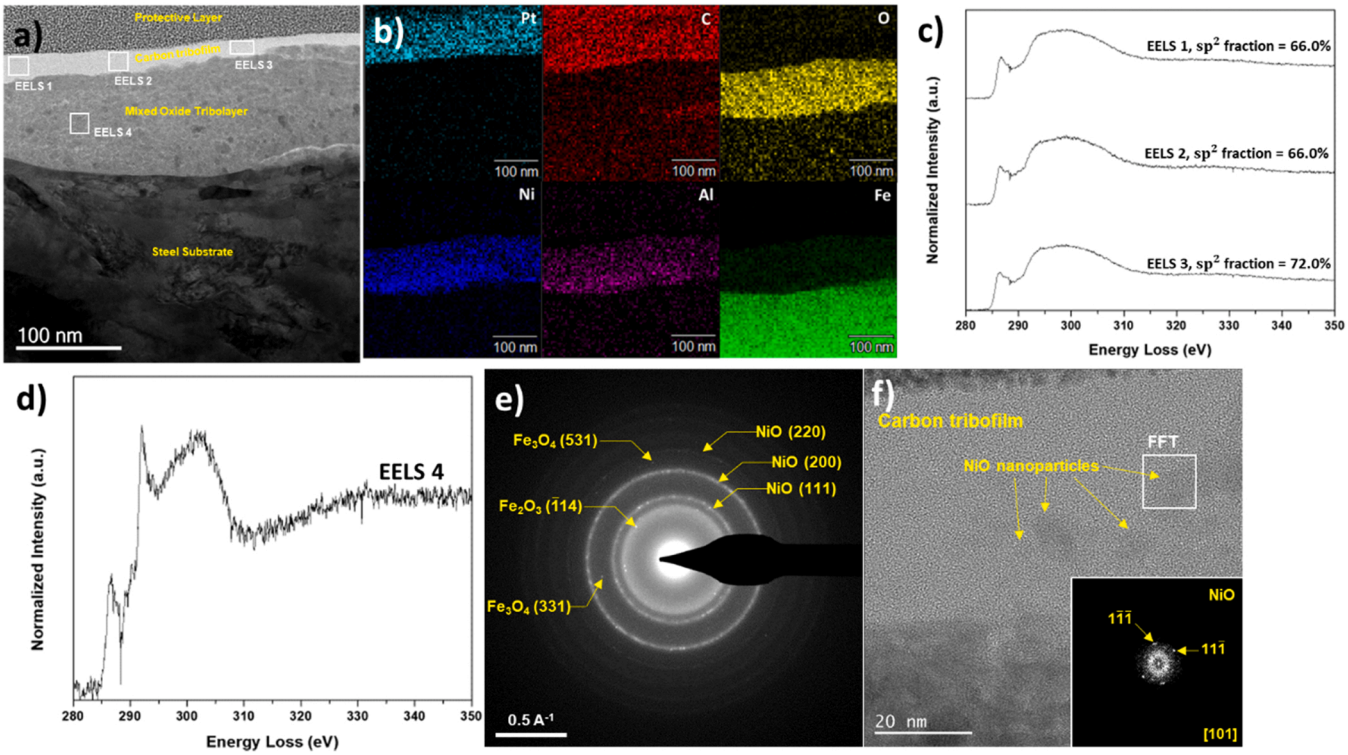

Fig. 8. (a) STEM-BF image of the tribofilm hierarchical structure; (b) STEM-EDS of the hierarchical tribofilm; (c) Core-loss EELS C-K edge of the top amorphous carbon layer; (d) Core-loss EELS C-K edge of the area in the mixed tribo-oxide layer; (e) SAED pattern of the mixed tribo-oxide layer; and (f) HR-TEM lattice imaging of the interface between the carbon and mixed oxide tribolayer. The cross-sectioned tribofilm was taken from the ball lubricated by CPCa+ 0.1%LDH lubricant under 10 N load at 50°C.

thermal decomposition process of NiAl-LDH also produces the Al_2O_3 phase which is amorphous [53]. Thus, the halo ring pattern of the amorphous phase in SAED could be attributed to the Al_2O_3 phase in the tribo-oxide layer. It is interesting to note that the core-loss EELS C-K edge taken in the tribo-oxide layer (Fig. 8d, EELS4) indicates a strong presence of sharp π * peak σ * molecular orbital transition peaks which is a characteristic of graphite. It is anticipated that when the LDH was oxidized during sliding at 50°C, the NiO phase formed and catalytically converted the disordered carbon on its surface, produced from the chemisorbed CPCa molecules, into graphitic carbon. A high fraction of sp^2 bonding in the top carbon tribofilm, 68%, could also be a result of the catalytic effect from the NiO phases being entrapped within the carbon film layer. High-resolution (HR)-TEM lattice imaging (Fig. 8f) indeed shows the presence of some NiO nanoparticles, evidenced by the FFT, in the carbon tribofilm, thus, further confirming the claim.

In the case of the tribofilm formed at 100°C, a slightly thinner superficial tribolayer (~15 nm) can be observed (Fig. 9a). This thin layer is wavy and is located above the fine-grain aggregate layer. The aggregate layer obtained after the test at 100°C is not densely compacted but rather loose compared to the one that resulted at 50°C. In addition, there is the presence of some low contrast and poorly crystalline domains within the aggregate layer. From the STEM-EDS (Fig. 9b), the top layer shows the high intensity of carbon which confirms the formation of the carbon tribofilm. Core-loss EELS analysis was also conducted in three different areas, denoted as EELS1, EELS2, and EELS3, showing the characteristic shape of amorphous carbon (Fig. 9c). Interestingly, the sp^2 fraction of this carbon tribofilm was calculated from the spectra taken at these areas (Fig. 8c) showing values between 71% and 83%. The average value of the sp^2 fraction in the carbon tribofilm obtained at 100°C is 79% which indicates a higher degree of graphitization compared to the one obtained at 50°C.

On the other hand, the fine grain aggregate tribo-layer beneath the carbon tribofilm still shows the strong intensity of elements from NiAl-LDH (Ni, Al, and O) and some intensity of Fe from steel (Fig. 9b). However, there is a different segregation of the elemental distribution compared to the fine-grain aggregate layer obtained at 50 °C. The fine grain aggregate layer comprises mostly Ni with some local areas of Al and Fe. Intriguingly, the O intensity only concentrates on the local areas of Al but not on Ni and Fe. It suggests that there were no or less oxides of Ni and Fe formation, and pure metallic Ni or Fe nanoparticles could be formed in the compacted tribo-layer. The SAED pattern of the fine-grain aggregate tribolayer beneath the carbon tribofilm and above the steel substrate shows powder diffraction ring patterns indexed to metallic Ni (Fig. 9d) with Ni (111) strongly diffracted. Thus, it can be concluded that the NiO was reduced into Ni during the friction test at 100 °C. Since Ni metal has been well-known as an active substrate for the growth of high graphitic carbon [54], the higher graphitic degree of the carbon tribofilm is expected if there are some Ni nanoparticles being entrapped in the carbon tribofilm. Indeed, the HR-TEM image indicates the presence of several metallic Ni nanoparticles, as indexed in FFT (Fig. 9e), in the carbon tribofilm. On the other hand, the Al- and O-rich areas shows interesting feature when compared to the Ni-rich areas. These areas are aluminium oxide and the diffraction contrast in the STEM-BF image (Fig. 9a) suggests these areas are amorphous. HR-TEM lattice imaging at the Al- and O-rich area shows a disordered and poorly crystalline structure with the presence of small crystalline domains. FFT from one small crystalline domain indicates the single crystalline of the α-Al_2O_3 phase. The in-situ chemical reduction of NiO into Ni during sliding and the formation and segregation of the semicrystalline Al_2O_3 have not been observed before and it will be discussed in detail in the following section.

4. Discussion

Forming the lubricous carbon tribofilms at the sliding contact has been recognized as a promising strategy to reduce friction and wear. Previous studies have demonstrated the ability to generate the carbon tribofilms during sliding by using the highly strained cycloalkane

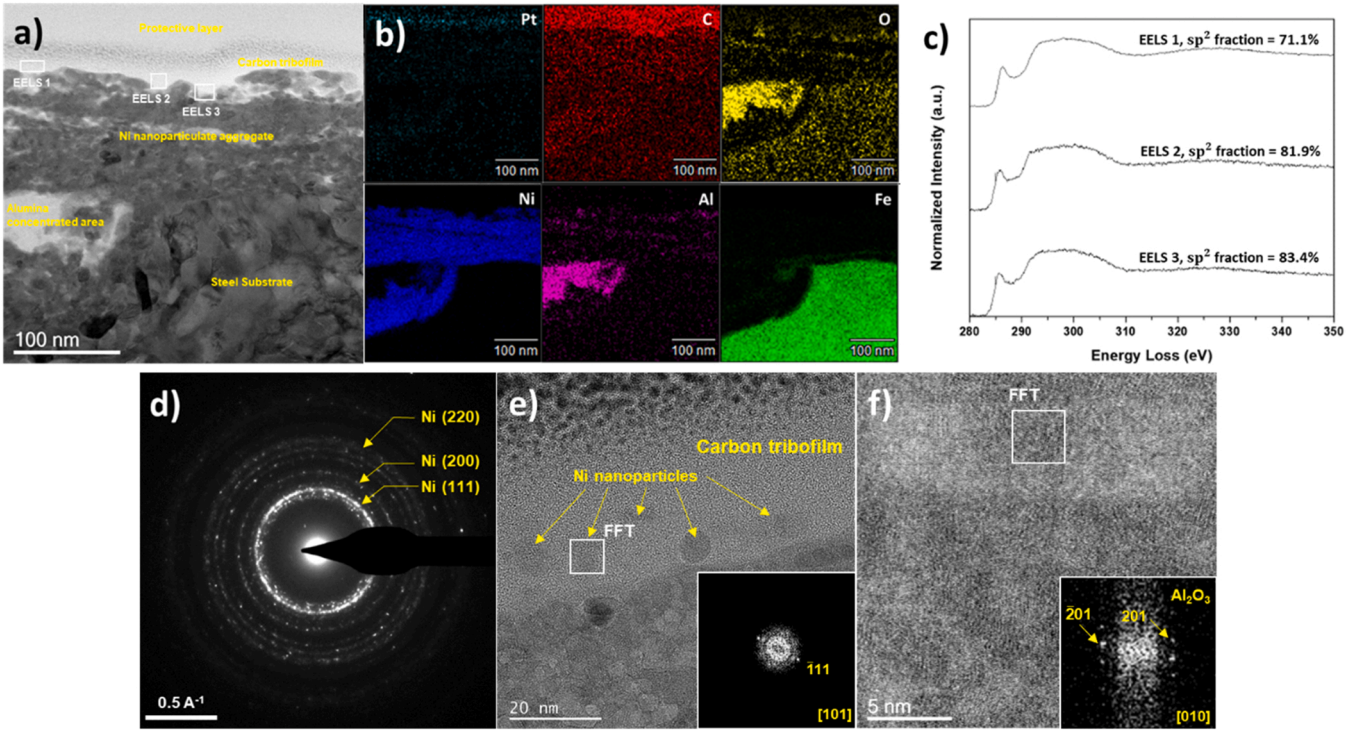

Fig. 9. (a) STEM-BF image of the tribofilm hierarchical structure; (b) STEM-EDS of the hierarchical tribofilm; (c) Core-loss EELS C-K edge of the top amorphous carbon layer; (d) high-resolution STEM lattice imaging of the Ni nano-particulate aggregate layer; (e) high-resolution STEM lattice imaging of the semi-crystalline Al_2O_3 area in the aggregate layer; and (f) high-resolution STEM lattice imaging at the interface between the aggregate layer and the steel substrate. The cross-sectioned tribofilm was taken from the ball lubricated by CPCa+ 0.1%LDH lubricant under 10 N load at 100°C.

carboxylic acids, e.g. CPCa, as the lubricant additive [21]. The carbon tribofilms, generated from these molecules by tribochemical processes, are polymeric and they can reduce friction and wear effectively at room temperature. From the results in this study, CPCa exhibited good friction reduction and anti-wear performance at 25 °C, however, the low-friction regime only retained for around 20 min. From the optical images (Fig. S5a), the non-uniform ball wear surface after lubricated by CPCa at 25 °C indicates the delamination of the tribofilm and the beneath tribo-oxide layer. Particularly, the dark grey areas, which show high Raman intensity of magnetite over hematite (Fig. S5b), are where the carbon tribofilm retained during sliding. The carbon tribofilm is expected to protect the sliding surfaces from oxidation and abrasive wear [21], thus, limiting the delamination of the tribo-oxide layer. Meanwhile, the white areas are where the carbon tribofilm was depleted, and these areas subsequently experienced the abrasive wear that delaminated the tribo-oxide layer to expose the pristine steel substrate. The Raman spectrum at the white areas, i.e. the ploughing at the white areas, shows higher intensity of hematite over magnetite (Fig. S5b) which indicates higher oxidation degree, thus, confirming the occurrence of more severe abrasive wear. The testing conditions in this study were at extreme lubrication regime ($\lambda = 0.08 << 1$) while those in the previous studies of CPCa were from moderate to mild boundary lubrication regime ($\lambda = 0.25–0.74 < 1$) [21,23]. Hence, it suggests that the polymeric carbon tribofilm produced from CPCa is not sufficiently stable to accommodate the significant mechanical stresses and shearing under severe boundary conditions.

4.1. Lubrication mechanism of the NiAl-LDH nanoparticles in synergy with the carbon tribofilm produced from CPCa at room temperature

We recognized that the addition of NiAl-LDH nanoparticles significantly improved the friction and wear performances of carbon tribofilm produced from CPCa across a broad temperature range (Figs. 3 and 5) under severe boundary conditions. At room temperature, the tribological improvement was mainly attributed to the key properties of NiAl-LDH as a typical layered 2D material. In particular, the initial reduction in friction during sliding (Fig. 3) could be attributed to the insertion of the LDH nanoparticles between the sliding interfaces and the wide cationic interlayer spacing (~0.75 nm) of the LDH (calculated from the XRD pattern in Fig. 2). While the presence of the LDH at the sliding interfaces prevented the direct asperities contact between the two surfaces, the wide interlayer spacing ensures the easy-exfoliation, thus, delivering an easy-shearing and slippage to the contacting surfaces [32,37]. It is expected that the LDH nanoparticles covered the entire contacting surfaces and formed the protective layer by their stacking which is characteristic of the layered materials at the sliding surfaces [55,56]. The CPCa molecules, initially physisorbed and chemisorbed on the LDH surfaces, might undergo friction-induced dissociation and polymerization to form the carbon tribofilm on top the protective LDH, i.e. the carbon tribofilm formed around the LDH nanoparticles.

The maximum flash temperature rise at the interface was calculated to be around 22.5°C for the testing conditions (see Supporting Information) which indicates the maximum temperature could reach ~ 50°C during sliding. This temperature is higher than the previous study testing conditions [21] that gave the interfacial maximum temperature up to 40°C (see Supporting Information). As the previous study could see the formation of thin carbon tribofilm [21], it is expected that the formation of the carbon tribofilm occurred in this study at 25°C. Therefore, the protective layer formed in these testing could comprise the carbon tribofilm on the LDH protective layer. Since both carbon tribofilms and LDH protective layer have been demonstrated to provide good anti-wear properties [30,57], the coverage of these films likle limits the abrasive wear resulting from the direct asperities contact or the formation of the third-body particles. The retaining of the magnetite-rich tribo-oxide layer, as evidenced by optical images in Fig. S2c and Raman spectrum in Fig. 7, confirms this assessment. This protective layer was able to support the load-carrying property up to 20 N which resulted in a slightly lower ball wear rate (equivalent to 1.59 GPa Hertzian contact pressure) (Fig. S3b). During sliding, this protective layer was sheared and gradually exfoliated by the asperities on the sliding surfaces. may explain the slight increase in the friction curve after approximately 35 min of sliding.

However, EDS analysis (Fig. 4c) suggests that this film did not absorb strongly on the sliding surfaces. No intensity of Ni and Al was found while there is a strong presence of O. The areas show no O signals in the EDS mapping in Fig. 4c could indicate the location where the protective layer presented predominantly during the friction test. Also, these areas appear more uniformly across the wear surfaces than the one from the CPCa tribotest (Fig. 4b), confirming the uniform distribution of the protective layer across the entire wear scar. This highlights the secondary role of CPCa in avoiding the agglomeration of the NiAl-LDH nanoparticles. We hypothesize that the disappearance of the protective layer was due to the deep cleaning process applied in this study. A similar observation was reported before for NiAl-LDH nano-additives when similar deep-cleaning processes of the ball samples were applied [55]. The deep cleaning process could wash off the nanoparticles physically lying on the wear scar. This removal processs by cleaning is reasonable for the NiAl-LDH nanoaparticles where the lubrication process at room temperature derives primarily from the layered structure [58,59] rather than the formation of the compact tribofilms from tribochemical reactions.

4.2. Lubrication mechanism of the NiAl-LDH nanoparticles in synergy with the carbon tribofilm produced from CPCa at high temperatures

At higher testing temperatures (50°C and 100°C), the lubricant became thinner which shifted the lubrication process into the more severe boundary lubrication regime. In such a condition, the collision between the asperities became more serious which generated more wear losses. This change is seen in the significant increase in the wear rate of the ball lubricated by CPCa at 50°C and 100 °C (Fig. 5b and 5d) compared to that at 25°C (Fig. 3). Fig. S5c, S5e show the relatively large wear scars on the balls after lubricating by CPCa at 50°C and 100°C with the presence of several ploughing and smearing areas. These observations indicate that severe abrasive wear occurred across the entire sliding surfaces which suggests the loss of protective function from carbon tribofilm produced from CPCa at these testing temperatures. We note that the carbon tribofilms were still formed at these temperatures as evidenced by the nano-scratch testing of the local areas on the wear surfaces which shows the lower friction of the C-film area compared to non C-film area (Fig. S6). A large variation in the friction curves at 50°C and 100°C (Fig. 5a and 5c) of CPCa lubricant was a consequence of the subsequent formation and removal of the carbon tribofilm during sliding. Since the carbon tribofilm was removed rapidly, it could not contribute the full protective effect and anti-friction property, thus, leading to severe surface oxidation and abrasive wear across the entire sliding surfaces.

Addition of 0.1 wt% NiAl-LDH markedly improved the friction and anti-wear performance of the CPCa lubricant at high temperatures. Along with the carbon film formation, the compact tribolayer formation also significantly contributed to the stable and low friction of CPCa+ 0.1%LDH lubricant compared to other additives. Local nano-scratch testing in Fig. S6 evidenced the lowest friction of the carbon tribofilm produced from this combination at two temperatures. The lowest and least fluctuation nano-friction curves at the carbon film areas of the CPCa+ 0.1%LDH is attributed to the higher degree of graphitization as demonstrated in Figs. 8c-d and 9c. More importantly, the improvement in anti-wear performance by 94% and 96% was observed at 50°C and 100°C, respectively which was comparable or even superior to the benchmark ZDDP additive (Fig. 5). Imaging of the wear morphology after nano-scratch testing (Table S7) also showed no obvious scratch marks of the tribofilm areas of this combination.

Notably, the wear rates of the balls lubricated by the CPCa+ 0.1%LDH lubricant at two different temperatures (50°C and 100°C) are approximately equal (Fig. 5b and 5d) which suggests the excellent anti-wear performance of this formulated package over the broad temperature range. The synergy between NiAl-LDH nanoparticles and CPCa may contribute to the outstanding lubrication results. According to the STEM characterization of the cross-section tribofilm, different tribofilm structures were observed, thus, indicating the different responses of CPCa and NiAl-LDH via temperature. The lubrication mechanism of such a combination can be understood by considering the thermal decomposition reactions of the LDH nanoparticles. Generally, the thermal decomposition of the NiAl-carbonate-LDH depends on the setting temperature [60]:

$$\left[Ni_{2/3}Al_{1/3}(OH)_2\right](CO_3)_{1/6}\cdot mH_2O \xrightarrow{25-250^{\circ}C} \left[Ni_{2/3}Al_{1/3}(OH)_2\right](CO_3)_{1/6} + mH_2O \quad (i)$$

$$2[Ni_{2/3}Al_{1/3}(OH)_2](CO_3)_{1/6} \xrightarrow{400-800^{\circ}C} 4\Big/3NiO.1\Big/3Al_2O_3 + 1\Big/3CO_2 + 2H_2O \quad (ii)$$

$$2[Ni_{2/3}Al_{1/3}(OH)_2](CO_3)_{1/6} \xrightarrow{>850^{\circ}C} NiO + 1\Big/3NiAl_2O_4 + 1\Big/3CO_2 + 2H_2O \quad (iii)$$

4.2.1. 50°C tribo-test condition

SAED analysis of the cross-section tribofilm at 50°C demonstrated the formation of the tribo-oxide layer comprising dominantly NiO and Al_2O_3 with minor presence of Fe_2O_3 and Fe_3O_4 (Fig. 8e). There is no detection of the $NiAl_2O_4$ phase in the SAED suggesting that the formation of this phase might not be formed at 50°C testing condition. As the intensity of Ni and Al distributed uniformly and in similar areas in the STEM-EDS mapping (Fig. 8b), we deduce that the thermal decomposition process of NiAl-LDH followed the chemical equation (ii). This assessment suggests that the friction testing condition at 50°C produces an effect equivalent to the static temperature heating at 400–800°C. However, the interfacial flash temperature rise was calculated for the testing conditions at 50°C (see Supporting Information) as 32°C, thus, the maximum temperature at the sliding interface could only reach 82°C. This implies that the interfacial pressure and the mechanical actions, e.g. stress-shearing and intermixing, contributed a critical role to the thermal decomposition of the NiAl-LDH nanoparticles [61].

In this case, previous work has demonstrated that Al_2O_3 phase both forms as a support phase on the surface of the NiO or as a Ni-doped separate phase surrounding the NiO [61]. A spinel-type $NiAl_2O_4$ phase could also be expected as a side product of the interaction between the NiO phase and Al_2O_3 support phase at high temperatures, but this phase is very poorly crystalline at lower than 850°C [53]. The presence of the $NiAl_2O_4$ phase can hinder the reduction of NiO phase into Ni and protect the alumina phase against the crystallization. However, the results at the 100°C friction test condition clearly demonstrate the formation of the Ni phase and the crystallization of the Al_2O_3 (Fig. 9f), thus, confirming no record of $NiAl_2O_4$ phase formation at either 50°C or 100°C testing conditions.

We interpret these results to reflect that the NiAl-LDH nanomaterials undergo thermal decomposition under the tribotest at 50°C, forming nanoparticles of NiO and Al_2O_3 at the sliding interface. During sliding, these oxide nanoparticles intermix with oxide debris, produced from the oxidation of the steel wear debris, and are compacted into the fine grain layer on the sliding surfaces. According to the Hall-Petch behaviour, the nanocrystalline layer provides a better yield strength which is a result of the grain-boundary strengthening effect [62]. Under friction conditions, the grain boundaries of the fine grain tribolayer can stop the propagation of cracks and dislocations while dissipating the frictional energy resulted from the plastic deformation of the near-surface steel matrix. Ultimately, the formation of the fine-grain oxide tribo-layer on the sliding surfaces could improve the tensile strength of the wear surfaces, reduce the sticking between the sliding counterparts, resulting in a stable friction regime with low wear damages [63]. The formation of the amorphous carbon tribofilm as the top layer follows thereafter when the tribo-oxide layer has already formed, attributable to the dissociation and polymerization of the CPCa molecules that physically absorb on the LDH nanoparticles. During sliding, these molecules easily detached from the NiAl-LDH nanoparticles when the nanoparticles undergo thermal decomposition and compaction into the tribo-oxide layer. Interfacial flash heating (maximum at 82°C) simultaneously with significant mechanical forces could induce the cracking of the highly strained cyclopropane into the radical carbons. These radical carbons polymerize under the support of the intermixing effect and stress-shearing energy to form the solid polymeric carbon film at the sliding interface [23].

Meanwhile, the fraction of the CPCa molecules chemically absorbed on the NiAl-LDH undergo chemical transformation into graphitic carbon during the thermal decomposition LDH nanoparticles by a friction process, as detected by EELS analysis in the tribo-oxide layer (Fig. 8d). The formation of the graphitic carbon around a NiO phase by calcining oleylamine-modified LDH at 300°C was observed previously and explained due to the catalytic effect of NiO [33]. However, the graphitic carbon formed on or around the NiO phase is not strongly crystalline which was shown by the HR-TEM lattice fringe in the previous study [33], suggesting that the structure of graphitic carbon was disordered and contained several defect active sites. The NiO nanoparticles emerging on the sliding surfaces may have disordered graphite around them. We hypothesize that the polymeric carbon tribofilm chemically connected to the oxide tribolayer via these defect active sites of the graphitic carbon appears on the NiO surface. Besides, some NiO nanoparticles presented within the carbon tribofilm, as suggested by HR-TEM lattice imaging and FFT (Fig. 8f), could catalytically graphitize part of the carbon tribofilm resulting in the high sp^2 bonding fraction (68 ± 3%). The higher degree of graphitization of the amorphous carbon film, the better the carbon film can accommodate shear-stress to reduce friction and wear [64]. Thus, the formation of the NiO-rich nano-grain tribo-oxide layer supports the formation of the stable and high-performance carbon tribofilm as suggested by distinct stable friction response and low wear rate even outperforming ZDDP tribofilm (Fig. 5a).

4.2.2. 100°C tribo-test condition

As the temperature increases to 100°C, the microstructure and composition of the tribofilm changes significantly. The reduction of NiO into Ni metallic nanoparticles across the tribofilm structure was confirmed by STEM-EDS and SAED analysis (Figs. 9b and 9d). Similar chemical reduction of the NiO into Ni was observed in the previous study of Wang et al. [33] for the oleylamine-modified NiAl-LDH nanoparticles which attribute to the presence of disordered graphitic carbon around the NiO phase. However, such a chemical reduction could only be triggered when the particles were calcined at 600°C and under vacuum or argon protection environments, i.e. in a depleted oxygen environment [33]. At the 100°C testing condition, the base lubricant (PAO-4) became thinner than at 50°C. At 100°C the lubrication regime is shifted toward the more severe boundary conditions where direct collision between the asperities on two sliding surfaces become more favourable. Consequently, the mechanical stresses and intermixing effect increase significantly and reduce the energy barrier for the chemical reduction of NiO into Ni. Meanwhile, the oxidation protection effect of the superficial carbon tribofilm produced from the tribo-induced dissociation and polymerization of CPCa may limit oxygen infiltration to the intermediate tribo-layer from surrounding air. Together, these conditions lead to the favourable reduction of the NiO particles into Ni nanoparticles by the disordered carbon around NiO and/or the H_2 generated from the dissociation of the CPCa molecules.

Owing to a high surface energy of the metallic nanoparticles [65,66],

they tend to agglomerate and sinter at high temperatures to reduce the surface area. The reduction of NiO into Ni followed by the aggregation of the Ni nanoparticles may drive the phase segregation of amorphous Al_2O_3 as seen in the STEM analysis (Fig. 9). The structure of the intermediate tribo-layer shows alternating Ni-rich nanoparticle aggregates and Al_2O_3-rich areas. The Ni-rich nanoparticle aggregates are loosely packed with the space between the Ni nanoparticles likely filled by amorphous Al_2O_3 (BF-STEM and STEM-EDS in Fig. 9a and 9b). In the large area of amorphous Al_2O_3, the formation of the nanocrystalline Al_2O_3 was observed (Fig. 9f), indicating a significant effect of the interfacial pressure and mechanical stresses under this condition on the tribo-chemical processes given that crystallization of amorphous Al_2O_3 to α-Al_2O_3 occurs at 1000–1050°C under isothermal annealing conditions [67].

In addition to the reduced thickness of the film at 100°C compared to the film produced at 50°C, the waviness of the carbon tribofilm follows the waviness of the Ni-rich fine-grain surface morphology (Fig. 9a). This structure suggests the carbon tribofilm was subsequently worn out and recovered following changes of the surface morphology. We hypothesize that the carbon tribofilm is initially formed from CPCa, and this carbon tribofilm contributes to the reduction of NiO to Ni as mentioned above. The film is subsequently delaminated and replenished by hydrocarbon from the PAO oil, due to the catalytic effect of pure metallic Ni nanoparticles [12] once CPCa is depleted. The high degree of graphitization of the carbon-based tribofilm produced at 100°C compared to 50°C, as calculated by the sp^2 bonding fraction, can be explained by the driving factors to graphitic probability P(s) of the generated carbon soot with large defects and sp^3 bonding according to the expression [68]:

$$P(s) = \exp\left(\frac{-(E - \sigma C)}{kT}\right) \quad (2)$$

where σ represents the applied stress of the system, k is the Boltzmann constant, C is a constant while E and T are the system's energy barrier and temperature, respectively. From this equation, increasing the temperature and reducing the activation barrier will increase the graphitic probability P(s) and result in a higher sp^2 bonding fraction in the carbon-based tribofilm. The maximum interfacial flash temperature produced at this tribo-test condition is 135°C (see Supporting Information). Meanwhile, the presence of Ni nanoparticles within the carbon tribofilm (Fig. 9f) can reduce the activation energy for the graphitization process [12]. The higher degree of graphitization of the carbon tribofilm can accommodate significant mechanical stresses and shearing produced at the 100°C testing conditions (Fig. 5) [69,70]. On the other hand, the fine-grain structure of the Ni-rich intermediate tribo-layer with the alternating presence of amorphous Al_2O_3 phase may also mitigate the destructive effect of the sliding-induced shear strain [71]. The amorphous-nanocrystalline structure exhibits improved strength and toughness properties, which avoids inhomogeneous structures appearing on the worn subsurface caused by the plastic deformation of multiple layers during the sliding process [71]. Taken together, the synergy between the highly graphitic carbon surface tribofilm and the nano-composite structure of the subsurface tribolayer provide a model for the astonishing stable friction and anti-wear performance comparable to ZDDP under tribo-test at 100°C.

Fig. 10 summarizes the lubrication mechanisms of the CPCa+ 0.1% LDH lubricant which results in the excellent anti-friction and anti-wear properties across 50–100°C temperatures.

5. Conclusion

In summary, comprehensive experiments have been carried out to evaluate the synergistic effect of layered double hydroxide in the lubrication of CPCa at different conditions. It has been found that 0.1 wt % addition of Ni-Al-LDH can improve remarkably the friction and wear performance of in-situ Carbon-based tribofilm CPCa under broad temperature range (25–100°C) under severe boundary lubrication conditions. While the lubrication mechanism at 25°C was attributed to the physical properties of LDH as 2D layered nanomaterial, the tribo-tests at higher temperatures showed the compact tribofilm formations via the tribochemical reactions. At 50°C, Ni-Al-LDH nanoparticles resulted in a nanocrystalline intermediate tribolayer containing rich $NiO.Al_2O_3$ phase that improved the mechanical properties of the sliding surfaces. As the temperature increased to 100°C, there was a reduction of the NiO phase into Ni nano-particulate along with the increase in graphitization of the upper carbon tribolayers. These unique hierarchical tribofilm formations, adapting to temperature, resulted in the significant wear reduction (by over 90%), and much stable and lower friction compared to that of pristine CPCa under severe boundary lubrication conditions. The anti-wear performance of these carbon-containing tribofilms showed comparable performance to ZDDPs at high temperatures. It is believed that this study will pave a pathway in the controlling the in-situ deposition of the durable and high-performance carbon-based tribofilm for harsh operation conditions in advanced engineering systems.

CRediT authorship contribution statement

Khai Kim Huynh: Investigation, Writing – original draft, Formal analysis, Data curation. **Sang T. Pham:** Conceptualization, Validation, Formal analysis, Writing – original draft, Visualization, Supervision. **Kiet A. Tieu:** Resources, Supervision, Project administration, Funding acquisition, Writing – review & editing. **Sean M. Collins:** Writing – review & editing, Funding acquisition. **Cheng Lu**: Supervision; Writing – review & editing. **Shanhong Wan:** Writing – review & editing.

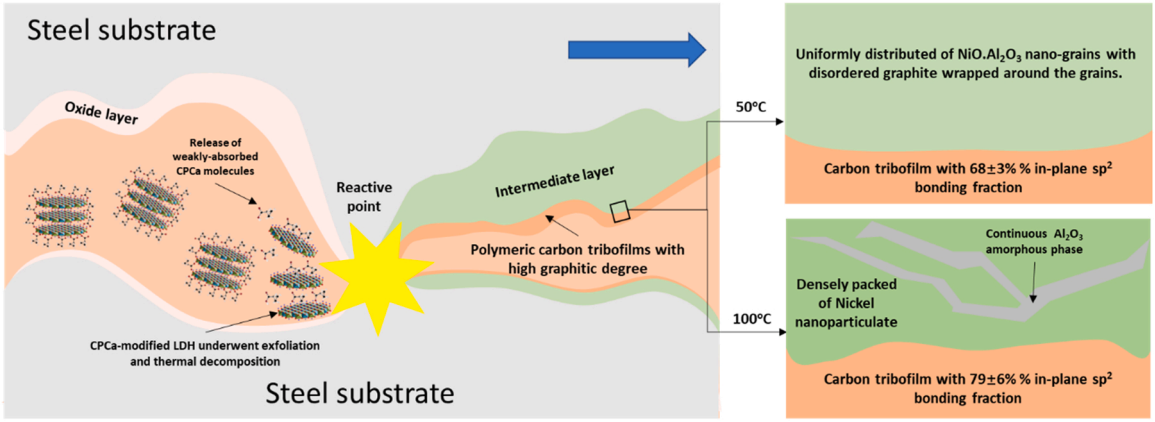

Fig. 10. Lubrication mechanisms of the CPCa+ 0.1%LDH lubricant.

Declaration of Competing Interest

The authors declare that they have no known competing financial interests or personal relationships that could have appeared to influence the work reported in this paper.

Data Availability

Data will be made available on request.

Acknowledgments

The study is funded by the Australian Research Council (ARC) Discovery Project DP190103455 and Linkage Project LP160101871. This study is also supported by Engineering and Physical Sciences Research Council – United Kingdom (Grant No. EP/V044907/1). The authors acknowledge the use of the JEOL JSM-6490LA and JEOL JSM-7500FA at the UOW Electron Microscopy Centre. The authors also gratefully acknowledge Dr. Zabeada Aslam in LEMAS at the University of Leeds for her support and assistance for using the Titan^3 Themis 300. The authors acknowledge the use of the Renishaw Raman from the LIEF grant LE 200100047. The authors are grateful for PhD student Tuong Ly Kiet Dao in providing support and assisting the synthesis of the LDH nanoparticles.

Associated Content

Calculation of maximum flash temperature rise and maximum temperature at the sliding inteface; The roughness variation of the disc wear track under different testing conditions; Friction and wear results of the CPCa+LDH lubricant at different testing conditions including different NiAl-LDH nanoparticles concentration and different normal loading conditions; Optical images and SEM-EDS analysis of the wear scar surfaces on the ball after the CPCa+LDH lubrication tests with at different Ni-Al-LDH nanoparticles concentration and different normal loading conditions; Optical images and Raman analysis of the wear scar surfaces on the ball after the lubrication test with CPCa at different temperatures.

Appendix A. Supporting information

Supplementary data associated with this article can be found in the online version at doi:10.1016/j.triboint.2023.108476.

References

[1] Wong VW, Tung SC. Overview of automotive engine friction and reduction trends–Effects of surface, material, and lubricant-additive technologies. Friction 2016;4:1–28.
[2] Holmberg K, Andersson P, Nylund N-O, Mäkelä K, Erdemir A. Global energy consumption due to friction in trucks and buses. Tribol Int 2014;78:94–114.
[3] Martinez JS, Hissel D, Pera M-C, Amiet M. Practical control structure and energy management of a testbed hybrid electric vehicle. IEEE Trans Veh 2011;60:4139–52.
[4] Tie SF, Tan CW. A review of energy sources and energy management system in electric vehicles. Renew Sust Energ Rev 2013;20:82–102.
[5] Kohlhauser B, Ripoll MR, Riedl H, Koller C, Koutna N, Amsüss A, et al. How to get noWear?–A new take on the design of in-situ formed high performing low-friction tribofilms. Mater Des 2020;190:108519.
[6] Esche C.K., Mazzamaro G.A., Bartels T., Gray D.B. Fuel efficient lubricating oils. Google Patents; 2017.
[7] Mazzamaro GA, Donnelly SG, Hiza RJ. Ultra low phosphorus lubricant composition. Google Pat 2014.
[8] Schmellenmeier H. Die Beeinflussung von festen Oberflachen durch eine ionisierte. Exp Tech Phys 1953;1:49–68.
[9] Al Mahmud K, Kalam MA, Masjuki HH, Mobarak H, Zulkifli N. An updated overview of diamond-like carbon coating in tribology. Crit Rev Solid State Mater Sci 2015;40:90–118.
[10] Vetter J. 60 years of DLC coatings: historical highlights and technical review of cathodic arc processes to synthesize various DLC types, and their evolution for industrial applications. Surf Coat Technol 2014;257:213–40.
[11] Taylor C. Automobile engine tribology—design considerations for efficiency and durability. Wear 1998;221:1–8.
[12] Erdemir A, Ramirez G, Eryilmaz OL, Narayanan B, Liao Y, Kamath G, et al. Carbon-based tribofilms from lubricating oils. Nature 2016;536:67–71.
[13] Aouadi SM, Gu J, Berman D. Self-healing ceramic coatings that operate in extreme environments: a review. J Vac Sci Technol A: Vac, Surf, Films 2020;38:050802.
[14] Shirani A, Gu J, Wei B, Lee J, Aouadi SM, Berman D. Tribologically enhanced self-healing of niobium oxide surfaces. Surf Coat Technol 2019;364:273–8.
[15] Berman D, Erdemir A. Achieving ultralow friction and wear by tribocatalysis: enabled by in-operando formation of nanocarbon films. ACS Nano 2021.
[16] Ramirez G, Eryilmaz OL, Fatti G, Righi MC, Wen J, Erdemir A. Tribochemical conversion of methane to graphene and other carbon nanostructures: implications for friction and wear. ACS Appl Nano Mater 2020;3:8060–7.
[17] Shirani A, Li Y, Eryilmaz OL, Berman D. Tribocatalytically-activated formation of protective friction and wear reducing carbon coatings from alkane environment. Sci Rep 2021;11:1–9.
[18] Xu X, Xu Z, Sun J, Tang G, Su F. In situ synthesizing carbon-based film by tribo-induced catalytic degradation of poly-α-Olefin oil for reducing friction and wear. Langmuir 2020;36:10555–64.
[19] Ma Q, Khan AM, Wang QJ. Dependence of tribological performance and tribopolymerization on the surface binding strength of selected cycloalkane-carboxylic acid additives. Tribol Lett 2020;68:1–10.
[20] Fu X, Cao L, Wan Y, Li R. Superlubricity achieved with TiN coatings via the in situ formation of a carbon-based film at the sliding interfaces. Ceram Int 2021;47:33917–21.
[21] Johnson B, Wu H, Desanker M, Pickens D, Chung Y-W, Wang QJ. Direct formation of lubricious and wear-protective carbon films from phosphorus-and sulfur-free oil-soluble additives. Tribol Lett 2018;66:2.
[22] Ta TD, Tieu AK, Tran BH. Influences of iron and iron oxides on ultra-thin carbon-based tribofilm lubrication. Tribol Int 2022:107665.
[23] Wu H, Khan AM, Johnson B, Sasikumar K, Chung Y-W, Wang QJ. Formation and nature of carbon-containing tribofilms. ACS Appl Mater Interfaces 2019;11:16139–46.
[24] Khan AM, Wu H, Ma Q, Chung Y-W, Wang QJ. Relating tribological performance and tribofilm formation to the adsorption strength of surface-active precursors. Tribol Lett 2020;68:1–9.
[25] Huynh KK, Tieu KA, Pham ST. Synergistic and competitive effects between zinc dialkyldithiophosphates and modern generation of additives in engine oil. Lubricants 2021;9:35.
[26] Wang H, Liu Y, Liu W, Wang R, Wen J, Sheng H, et al. Tribological behavior of NiAl-layered double hydroxide nanoplatelets as oil-based lubricant additives. ACS Appl Mater Interfaces 2017;9:30891–9.
[27] Rives V. Layered double hydroxides: present and future: Nova Publishers; 2001.
[28] Wang H, Wang Y, Liu Y, Zhao J, Li J, Wang Q, et al. Tribological behavior of layered double hydroxides with various chemical compositions and morphologies as grease additives. Friction 2021;9:952–62.
[29] Dao TLK, Tieu AK, Tran BH, Pham ST. Influence of structural disorders on the tribological behavior of phosphate-intercalated layered double hydroxide additives in polyalphaolefin. Langmuir 2022.
[30] Zhou C, Li Z, Liu S, Zhan T, Li W, Wang J. Layered double hydroxides for tribological application: recent advances and future prospective. Appl Clay Sci 2022;221:106466.
[31] Williams GR, O'Hare D. Towards understanding, control and application of layered double hydroxide chemistry. J Mater Chem 2006;16:3065–74.
[32] Xiao H, Liu S. 2D nanomaterials as lubricant additive: a review. Mater Des 2017;135:319–32.
[33] Wang H, Liu Y, Guo F, Sheng H, Xia K, Liu W, et al. Catalytically active oil-based lubricant additives enabled by calcining Ni–Al layered double hydroxides. J Phys Chem Lett 2019;11:113–20.
[34] Hu J, Zhang Y, Yang G, Gao C, Song N, Zhang S, et al. In-situ formed carbon based composite tribo-film with ultra-high load bearing capacity. Tribol Int 2020;152:106577.
[35] Mishra G, Dash B, Pandey S. Layered double hydroxides: a brief review from fundamentals to application as evolving biomaterials. Appl Clay Sci 2018;153:172–86.
[36] Evans DG, Slade RC. Structural aspects of layered double hydroxides. Layer Double Hydroxides 2006:1–87.
[37] Dao TLK, Tieu KA, Tran BH. Tribochemical synergy between phosphate-intercalated layered double hydroxide additives and super high oleic safflower oil on sliding contacts. Phys Chem Chem Phys 2022;24:20282–93.
[38] Pham ST, Tieu AK, Wan S, Hao J, Zhu H, Nguyen HH, et al. Oxidative and frictional behavior of a binary sodium borate–silicate composite in high-temperature lubricant applications. Ind Eng Chem Res 2019;59:2921–33.
[39] Hamrock B.J., Dowson D. Isothermal elastohydrodynamic lubrication of point contacts: part III—fully flooded results. 1977.
[40] Faour A, Mousty C, Prevot V, Devouard B, De Roy A, Bordet P, et al. Correlation among structure, microstructure, and electrochemical properties of NiAl–CO_3 layered double hydroxide thin films. J Phys Chem C 2012;116:15646–59.
[41] Liu Y, Yu T, Cai R, Li Y, Yang W, Caro J. One-pot synthesis of NiAl–CO 3 LDH anti-corrosion coatings from CO 2-saturated precursors. RSC Adv 2015;5:29552–7.
[42] Stachowiak GW. Particle angularity and its relationship to abrasive and erosive wear. Wear 2000;241:214–9.
[43] Roberts A, Brooks R, Shipway P. Internal combustion engine cold-start efficiency: a review of the problem, causes and potential solutions. Energy Convers Manag 2014;82:327–50.
[44] Will F. Fuel conservation and emission reduction through novel waste heat recovery for internal combustion engines. Fuel 2012;102:247–55.

[45] Will F, Boretti A. A new method to warm up lubricating oil to improve the fuel efficiency during cold start. SAE Int J Engines 2011;4:175–87.
[46] André M. In actual use car testing: 70,000 kilometers and 10,000 trips by 55 French cars under real conditions. SAE Trans 1991:65–72.
[47] Erdemir A, Ramirez G, Eryilmaz OL, Narayanan B, Liao Y, Kamath G, et al. Carbon-based tribofilms from lubricating oils. Nature 2016;536:67–71.
[48] Pham ST, Wan S, Tieu KA, Ma M, Zhu H, Nguyen HH, et al. Unusual competitive and synergistic effects of graphite nanoplates in engine oil on the tribofilm formation. Adv Mater Interfaces 2019;6:1901081.
[49] Miranda AM, Castilho-Almeida EW, Ferreira EHM, Moreira GF, Achete CA, Armond RA, et al. Line shape analysis of the Raman spectra from pure and mixed biofuels esters compounds. Fuel 2014;115:118–25.
[50] Li Y.-S., Jang S., Khan A., Martin T., Wang Q.J., Martini A., et al. Do DLC-like features in Raman spectra of tribofilms really mean they are DLC formed by friction? 2022.
[51] Chen X, Zhang C, Kato T, Yang X-A, Wu S, Wang R, et al. Evolution of tribo-induced interfacial nanostructures governing superlubricity in aC: H and aC: H: Si films. Nat Commun 2017;8:1–13.
[52] Lanigan J, Freeman HM, Wang C, Ward MB, Morina A, Neville A, et al. Understanding the wear behaviour of non-doped and Si, O-doped diamond-like carbon films. RSC Adv 2017;7:43600–10.
[53] Clause O, Rebours B, Merlen E, Trifiro F, Vaccari A. Preparation and characterization of nickel-aluminum mixed oxides obtained by thermal decomposition of hydrotalcite-type precursors. J Catal 1992;133:231–46.
[54] Bokhonov B, Korchagin M. The formation of graphite encapsulated metal nanoparticles during mechanical activation and annealing of soot with iron and nickel. J Alloy Compd 2002;333:308–20.
[55] Wang H, Liu Y, Chen Z, Wu B, Xu S, Luo J. Layered double hydroxide nanoplatelets with excellent tribological properties under high contact pressure as water-based lubricant additives. Sci Rep 2016;6:1–8.
[56] Tang G, Wu Z, Su F, Wang H, Xu X, Li Q, et al. Macroscale superlubricity on engineering steel in the presence of black phosphorus. Nano Lett 2021;21:5308–15.
[57] Argibay N, Babuska T, Curry J, Dugger M, Lu P, Adams D, et al. In-situ tribochemical formation of self-lubricating diamond-like carbon films. Carbon 2018;138:61–8.
[58] Wang H, Liu Y, Liu W, Liu Y, Wang K, Li J, et al. Superlubricity of polyalkylene glycol aqueous solutions enabled by ultrathin layered double hydroxide nanosheets. ACS Appl Mater Interfaces 2019;11:20249–56.
[59] Hilton MR, Bauer R, Didziulis SV, Dugger MT, Keem JM, Scholhamer J. Structural and tribological studies of MoS2 solid lubricant films having tailored metal-multilayer nanostructures. Surf Coat Technol 1992;53:13–23.
[60] Sato T, Fujita H, Endo T, Shimada M, Tsunashima A. Synthesis of hydrotalcite-like compounds and their physico-chemical properties. React Solids 1988;5:219–28.
[61] Tysoe W. On stress-induced tribochemical reaction rates. Tribol Lett 2017;65:1–16.
[62] Farhat Z, Ding Y, Northwood D, Alpas A. Effect of grain size on friction and wear of nanocrystalline aluminum. Mater Sci Eng: A 1996;206:302–13.
[63] Pham ST, Tieu KA, Wan S, Lei W, Liu D, Tran NV. Anti-oxidation mechanism and interfacial chemistry of BN@ CaCO3-SiO2 microcapsule-added sodium borate melt on the sliding steel surfaces at elevated temperatures. Appl Surf Sci 2021;566:150556.
[64] Wei C, Wang Y-S, Tai F-C. The role of metal interlayer on thermal stress, film structure, wettability and hydrogen content for diamond like carbon films on different substrate. Diam Relat Mater 2009;18:407–12.
[65] Vitos L, Ruban A, Skriver HL, Kollár J. The surface energy of metals. Surf Sci 1998;411:186–202.
[66] Campbell CT, Parker SC, Starr DE. The effect of size-dependent nanoparticle energetics on catalyst sintering. Science 2002;298:811–4.
[67] Boumaza A, Favaro L, Lédion J, Sattonnay G, Brubach J, Berthet P, et al. Transition alumina phases induced by heat treatment of boehmite: an X-ray diffraction and infrared spectroscopy study. J Solid State Chem 2009;182:1171–6.
[68] Hoffman EE, Marks LD. Graphitic carbon films across systems. Tribol Lett 2016;63:1–21.
[69] Zhang R, Chen Q, He Z, Xiong L. In situ friction-induced amorphous carbon or graphene at sliding interfaces: effect of loads. Appl Surf Sci 2020;534:146990.
[70] Shirani A, Li Y, Smith J, Curry J, Lu P, Wilson M, et al. Mechanochemically driven formation of protective carbon films from ethanol environment. Materials Today. Chemistry 2022;26:101112.
[71] Liu C, Li Z, Lu W, Bao Y, Xia W, Wu X, et al. Reactive wear protection through strong and deformable oxide nanocomposite surfaces. Nat Commun 2021;12:1–8.